Physica Scripta. Vol. T110, 379–383, 2004

Fully Differential Study of Transfer Ionization Processes—a View into Correlated Many Particle Dynamics

Lothar Ph. H. Schmidt[1], Feras Afaneh[2], M. Schöffler[1], J. Titze[1], O. Jagutzki[1], Th. Weber[1], K. E. Stiebing[1], R. Dörner[1] and H. Schmidt-Böcking[1]

[1] Institut für Kernphysik, Universität Frankfurt, August-Euler-Str. 6, 60486 Frankfurt, Germany
[2] Physics Department, Hashemite University, Zarqa 13115, Jordan

PACS ref: 34.70.+e; 34.50.Fa

Received August 28, 2003; accepted November 21, 2003

Abstract

Using Cold target recoil Ion momentum spectroscopy (COLTRIMS) we have investigated the production of one free electron in slow $He^{2+} + He(1s^2)$ collisions. Kinematically complete data have been measured for all possible final states of the second electron, which is either still bound at the target or transferred to the projectile. The result will be discussed within the molecular orbital approach. Strong correlation between the bound electron final state and the electron emission pattern has been observed. This shows that the description of the electron emission from multi electron systems by a single active electron approach is not sufficient.

1. Introduction

Impressive theoretical progress was made in the treatment of electron transfer reaction in slow collisions. One example is the successful prediction of the population of even highly excited states in He^{2+}–He collisions by the semiclassical close-coupling method [1]. Within the semiclassical approach a theoretical description of such a collision process has to answer the question, of how the two-electron wave function develops in the time dependent two-center coulomb potential, given by the motion of the nuclei. This electronic wave function is in the molecular orbital approach represented in a basis of molecular Eigenstates, which is continuously adapted to the changing inter nuclear axis. Within this approach satisfactory results for the resonant double electron capture ($He^{2+} + He(1s^2) \rightarrow He(1s^2) + He^{2+}$) can be achieved by using only three molecular basis states [2]. Since the single electron capture is related to the population of other molecular states, these have to be included into the basis, but also those calculation are feasible since the late seventies [3]. In the more recent work of Gao *et al.* [4] a fully quantum-mechanical molecular-orbital treatment using the Born–Oppenheimer approximation was used to achieve agreement between theoretical and experimental results for the single differential cross section, also at very small scattering angles.

In spite of the success of the close coupling method in describing reactions where all electrons end up in bound states, electron emission to the continuum in slow collisions was not sufficiently considered so far. This is in contrast to the importance of this reaction channel. The total cross sections for the transfer ionization (TI)

$$He^{2+} + He \rightarrow He^{+} + e^{-} + He^{2+} \quad (1)$$

and the single ionization (SI)

$$He^{2+} + He \rightarrow He^{2+} + e^{-} + He^{+} \quad (2)$$

processes were experimentally found to be in the range of $10^{-17}\,cm^2$ [5,6] at $v_p = 1$ a.u. projectile velocity (25 keV/u). This is only a factor of 0.4 smaller than the total cross section for single capture to the ground state (SC1: $He^{2+} + He \rightarrow He^{+}(1s) + He^{+}(1s)$).

In slow collisions the production of free electrons can not in contrast to electrons transfer be treated perturbatively and the time dependence of the ionization has to take into account. In classical-trajectory-Monte Carlo (CTMC) calculations [7] for p + H collisions, Olson *et al.* found electrons emitted in the forward direction with nearly half of the projectile velocity. Olson *et al.* assumed that *these electrons are left stranded equidistantly between the projectile and target nuclei by the balance of the attractive Coulomb forces of both ions* [8]. The velocity of the saddle point (SP) of the two center coulomb potential of the nuclei depends on the charge of the projectile and the target nucleus, respectively. In the late 1980's several measurements at collision energies between 50 and 100 keV/u were done at Rolla [9,10] and Bariloche [11,12] in searches for the SP mechanism. These experiments, using dispersive electron spectrometers, yielded conflicting results. Only the Rolla group claimed evidence of the SP mechanism from their data.

Within the semi classical molecular orbital approach, the Hidden-crossing [13] model can be used to evaluate the probability of electron emission in slow p + H collisions. It describes the promotion to the continuum as an infinite series of transitions between H_2^+ Eigenstates at continuously increasing internuclear distances. The spatial expansion of the collision system causes excitation of the H_2^+ quasi molecule by radial coupling between states of the same molecular symmetry. The representation of the electron wave function by adiabatic states does represent the expansion of the system at coordinate space but does not consider the associated spread of the electron momentum distribution correctly. Therefore the final state electron momentum distribution can not be described. Nevertheless the angular distribution of the electrons at the plane perpendicular to the beam direction, which also is the final state inter nuclear axis, is defined by the symmetry of the molecular states, involved in the hidden crossing promotion.

The first experiment, where the electron momentum pattern was imaged in respect to the nuclear scattering plane was performed by Dörner *et al.* [14]. They discovered a two-finger structure in momentum space with a node on the saddle, which has been interpreted as a

strong π state contribution for the SI is $p + He$ collision [15]. Further experiments with similar setups had been reported by Abdallah *et al.* [16–18] and Afaneh [19] using He^+-, He^{2+}- and Ne^+- ions as projectiles and He and Ne as targets. In the present work we focus on the He^{2+}, He collision system. In addition to the rotational symmetry with respect to the internuclear axis the electronic Hamiltonian as well as the He_2^{2+} molecular states uses by the molecular orbital approach are symmetric with respect to the molecular center. Furthermore the mirroring of the system at the molecular center exchanges the final states of the SI and the TI. This feature makes this system well suited for the analysis within the molecular orbital approach.

2. Experimental setup

The experimental method was based on the Cold Target Recoil Ion Momentum Spectroscopy (COLTRIMS) [20,21]. A well-localized reaction zone of approximately $1\,mm^3$ is defined by the overlap of a collimated projectile beam and a internal cold supersonic gas jet crossing at 90°. Perpendicular to the projectile and the gas beams the ionized target atoms and the emitted electrons are extracted by a weak electric field in opposite directions onto two multi channel plate detectors. The momentum vector of these both fragments can be calculated from the times-of-flight and the positions on the detectors.

The gas jet consists of two stages. He at 17 bar is expanded through a 0.03 mm nozzle into the first expansion chamber, which is at a pleasure of 10^{-1} mbar and pumped by a $200\,m^2/h$ roots pump. 3 mm behind the nozzle a small part of the supersonic expansion is cut out by a 0.3 mm skimmer and transmitted into the second expansion chamber, which is at $5 \cdot 10^{-5}$ mbar. A second skimmer of 0.4 mm diameter is placed in a distance of 30 mm from the nozzle and separates the second chamber from the reaction chamber. This setup provides a gas jet of 1.1 mm diameter at the overlap with the projectile beam. The target density was estimated from the gas flow into the jet catcher to be $2{\cdot}10^{11}\,cm^{-2}$ while the residual gas density at the reaction chamber is $2{\cdot}10^{9}\,cm^{-3}$. The mean momentum of the He atoms in the jet of 6 a.u. and the divergence of 10 mrad gives a momentum spread of the gas target of 0.07 a.u. in the plane perpendicular to the jet direction. In the jet direction the momentum spread was estimated from the speed ratio [22] to be 0.25 a.u.

At the target region a homogeneous electric field is applied perpendicular to the plane defined by the projectile beam (z-axis) and gas jet (y-axis). This field projects the ionized target ions and the electrons in opposite directions on to two micro channel plate detectors with delay line anodes aligned in the y, z plane. The electron part of the spectrometer consists of a 13 mm field region and a 26 mm drift (Wiley–McLaren condition), which are separated by a grid of 80% transmission with 0.25 mm mesh size.

The electron detector has an active area of 80 mm and is shifted by 20 mm forward in beam direction with respect to the reaction zone. Beside this shift the spectrometer is cylindrical symmetric to the x-axis, which is defined by the electric field direction and originated at the reaction volume. The electric field was adjusted between 0.4 V/mm and 0.8 V/mm to get electrons emitted in beam direction with 1.1 times the projectile velocity v_p at the front edge of the detector. Thereby the electron velocity range of v_p is spread over 55 mm at the detector. For a typical field of 0.6 V/mm electrons with zero momentum have a time of flight of 30 ns with a slope of the time to velocity calibration function of 0.05 a.u. momentum per 1 ns.

The reaction time was determined either by detecting the charge state modified projectiles with a precession of 1.5 ns or by a trigger signal of a beam pulser with 2.5 ns pulse length and 4 MHz repetition rate. For the typical spectrometer field the related (x, y, z) electron velocity resolution (FWHM) is $(0.07, 0.1, 0.07)v_p$ for measurements with projectile detector and $(0.08, 0.17, 0.08)v_p$ for the pulsed beam experiments.

The recoil ions are created with less than 50 meV kinetic energy. Hence after passing a few cm extraction field the ions are quasi mono energetic. Common electrostatic ion beam optic can then be used to optimize the characteristics of the recoil ion spectrometer. A combination of a lens and a drift region is sufficient, to make the position on the detector as well at the time of flight nearly independent on the spread of the reaction volume (three-dimensional position and time focusing [23,24]). Caused by the acceleration of the recoil ions at the lens, which is embedded in the acceleration field, the ratio between field and drift region has to be larger than the factor 2 of the Wiley–McLaren geometry, which was used for the electrons. By using the SIMION program the geometry of the electrodes which define the electric field had been optimized (for a sketch of the spectrometer, see Fig. 1). The distance between target and recoil ion detector is 355 mm. For a typical extraction field of 0.6 V/mm the resolution of the recoil momentum in the projectile beam direction (z) was 0.2 a.u. The transversal resolution was limited to 0.4 a.u. (FWHM) by the broader momentum distribution of the gas target in the jet direction and electronic problems in the recoil flight times measurement.

3. Kinematics of electron transfer and ionization

The final state projectile momentum is not measured, but is calculated from the ion and electron momenta using momentum conservation. Therefore the kinematically complete information is available and the energy conservation determines the electron binding energy of the He^+ ion in the final state with an accuracy of 10 eV (FWHM). As a consequence of the conservation laws, the change of electronic binding energy is mainly reflected in the longitudinal momentum of the recoil ion $p_{z,\mathrm{rec}}$. Accounting only the leading terms of the kinetic energy, for the transfer of m electrons, $p_{z,\mathrm{rec}}$ can be calculated from the Q-value, which is the change of binding energies ($Q > 0$ if the electrons gets stronger bound) as

$$p_{z,\mathrm{rec}} = -\frac{Q}{v_p} - m\frac{m_e v_p}{2} \tag{3}$$

(see [20,23]). Figure 2(a) shows the $p_{z,\mathrm{rec}}$ distribution for single electron capture ($m = 1$) at $He^{2+} + He$ collisions

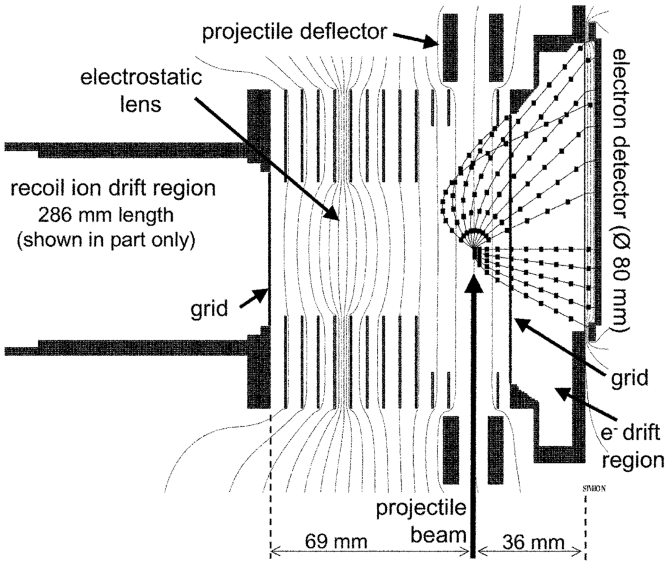

Fig. 1. Sketch of the spectrometer (the recoil ion drift region is only partly shown): For an electrostatic field at the reaction zone of 0.9 V/mm electron trajectories had been calculated using the SIMION program. The electrons emitted to the upper part with angles of $-75°$, -60, $-45°, \ldots, 75°$ to the beam directions have 13.6 eV energy. At the lower part the electrons are emitted in opposite to the beam directions with 0, 0.05, 0.1, 0.15, 0.2 a.u. momentum. The small squares at the trajectories mark the electrons positions at 2.5, 5, 7.5, ... ns time of flight.

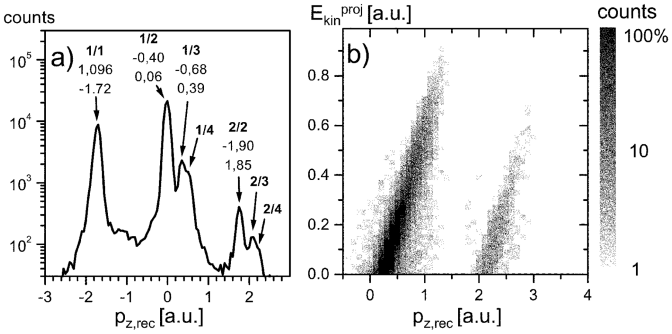

Fig. 2. Recoil ion longitudinal momentum $p_{z,\mathrm{rec}}$ distributions at $v_\mathrm{p} = 0.84$ a.u.: (a) SC at He^{2+} He collisions. The peaks are related to certain final state binding energies. The peaks are labeled with (top down): main quantum numbers of the two He^+ fragments, Q-value, $p_{z,\mathrm{rec}}$ calculated with Eq. (3). (b) Transfer ionization electron kinetic energy in the rest frame of the projectile $E_\mathrm{kin}^\mathrm{proj}$ as a function of $p_{z,\mathrm{rec}}$.

with $v_p = 0.84$ a.u. The possible Q-values of this reaction are given by the main quantum numbers of the recoil (n_rec) and the projectile (n_proj) ion as

$$Q = -2.9\,\mathrm{a.u.} + 2\,\mathrm{a.u.}\left(\frac{1}{n_\mathrm{rec}^2} + \frac{1}{n_\mathrm{proj}^2}\right). \tag{4}$$

The L and M shells, which differ by 7.6 eV are well separated and even the N shell can be identified as shoulder at the M shell peak. The peaks at $p_{z,\mathrm{rec}} > 1.5$ a.u. are related to single electron capture channels with simultaneous excitation of both He^+ fragments.

At TI and SI $p_{z,\mathrm{rec}}$ has to balance also the longitudinal (z) momentum of the free electron $p_{z,\mathrm{e}}$. Furthermore the electron kinetic energy E_kin leads to an additional deceleration of the projectile which has to be considered at the momentum balance [20,23].

$$p_{z,\mathrm{rec}} = -\frac{Q}{v_\mathrm{p}} - m\frac{m_\mathrm{e} v_\mathrm{p}}{2} + \frac{E_\mathrm{kin}}{v_\mathrm{p}} - p_{z,\mathrm{e}}. \tag{5}$$

The two additional contributions to this formula, which consider the free electron, can be merged by expressing the electron kinetic energy in the rest frame of the projectile $E_\mathrm{kin}^\mathrm{proj}$ instead of the laboratory frame:

$$p_{z,\mathrm{rec}} = -\frac{Q}{v_\mathrm{p}} - (m+1)\frac{m_\mathrm{e} v_\mathrm{p}}{2} + \frac{E_\mathrm{kin}^\mathrm{proj}}{v_\mathrm{p}}. \tag{6}$$

Figure 2(b) shows for TI at $v_\mathrm{p} = 0.84$ a.u. two well separated areas, which can be related to the K and L shell He^+ projectiles. The same identification of the He^+ electronic state is possible for the SI, where the bound electron is located at the the recoil ion. The binding energy of the He^+ fragment was used to subdivide the TI (as well as SI) into TI1 (SI1) for $He^+(1s)$ and TI2 (SI2) for those reactions, where the bound electron is excited.

4. Results

At these low impact velocities the transverse momentum exchange between target nucleus and projectile by far dominates over the momentum transfer to the electron (see discussion below and [20]). Therefore for the electron transfer reactions as well as the electron emission the momentum transfer to the recoil ion provides information about the impact parameter and the energy exchanged between the nuclear motion, the electronic binding energy and electron kinetic energy. For the TI1, where one electron is transferred to the K shell of the projectile, Fig. 3 shows the recoil ion momentum distribution. Most of the events are found at a broad distribution of

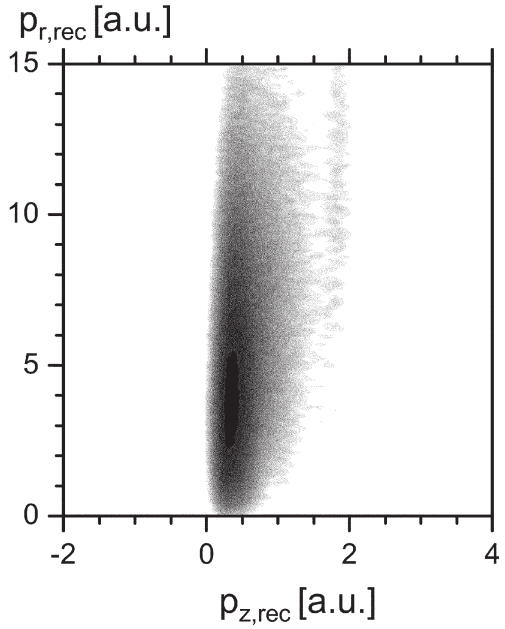

Fig. 3. Two dimensional recoil ion momentum distribution $\mathrm{d}^2\sigma/(\mathrm{d}p_{z,\mathrm{rec}}\,\mathrm{d}p_{r,\mathrm{rec}})$ for the TI1 (bound electron in 1s state): $p_{z,\mathrm{rec}}$ is the momentum in direction of the incoming projectile beam and reflects the electron kinetic energy in respect to the projectile frame. The sharp line structure at $p_{z,\mathrm{rec}} = 2$ a.u. is related to the autoionizing double electron capture, which leads to electrons emitted with approximately 35 eV from the projectile. $p_{r,\mathrm{rec}}$ is the recoil ion momentum transversal to the beam direction which is related to the inverse impact parameter.

longitudinal momenta $p_{z,\mathrm{rec}}$ between 0 and 1 a.u. There is no obvious correlation between $p_{z,\mathrm{rec}}$ and the transversal momentum $p_{r,\mathrm{rec}}$, which reflects the inverse impact parameter. At longitudinal momentum above 2 a.u. the transfer ionization with excitation of the projectile (TI2) is located (see Fig. 2). Nevertheless also the TI1 has a sharp line structure in this region. The well defined $p_{z,\mathrm{rec}}$ of these events indicate, that they are related to a primary capture process with the electron emitted by a second step not affecting the recoil ion momentum. According to Eq. (6) electrons of fixed $p_{z,\mathrm{rec}}$ have a certain energy with respect to the projectile frame $E_{\mathrm{kin}}^{\mathrm{proj}}$, which is here approximately 35 eV. Such electron energies are much higher than those expected for electrons emitted by the saddle point mechanism res. the hidden crossing promotion. While low energetic electrons are detected with 4π, the spectrometer accepts them only within the geometrical solid angle of the detector. These fast electrons are produced by the auto ionizing double electron capture (ADC) to $He(2p^2)$ or (2s,2p) [25].

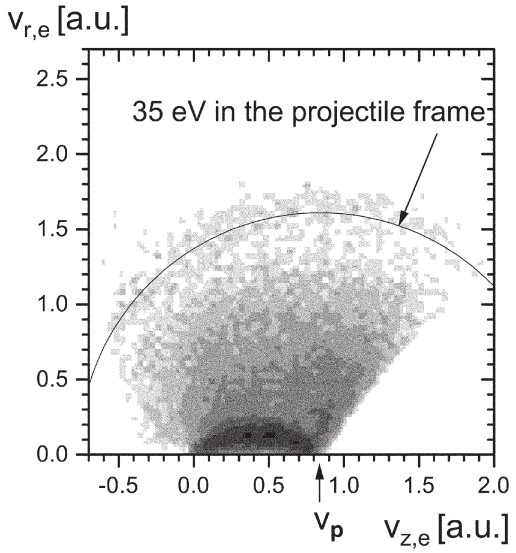

Fig. 4. Two dimensional electron velocity distribution $d^2\sigma/(dv_{z,e}\ dv_{r,e})$ for the TI1 (bound electron in 1s state): electrons emitted in direction of the electron detector. The circular arc marks the locus of electrons emitted from the projectile with approximately 35 eV.

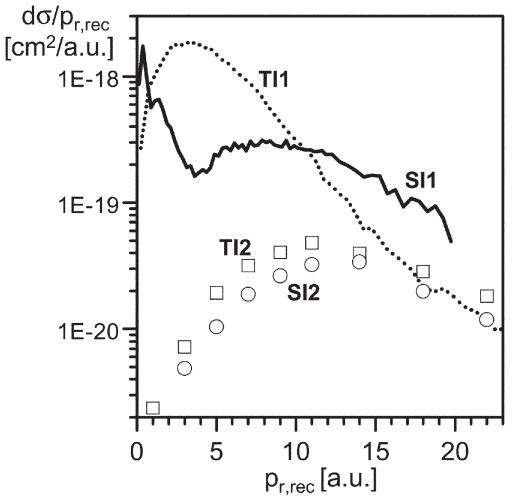

Fig. 5. Single differential cross sections $d\sigma/dp_{r,\mathrm{rec}}$ of SI1 (full line), TI1 (dashed line) SI2 (circles) and TI2 (squares) at projectile velocity $v_p = 0.9$ a.u.

Figure 4 shows the two dimensional electron velocity distribution parallel and perpendicular to the projectile beam. Most electrons are found at transverse momenta $p_{r,e} = m_e\ v_{r,e} < 0.3$ a.u. This is much less than the typical momentum transfer to the recoil ion, which is mainly caused by the nuclear repulsion. Within the semi classical approximation the nuclear motion approximately takes place in a plane. This plane will be used to define an internal reference frame (x', y', z') of the reaction with the z'-axis still in direction of the incoming projectiles, the x'-axis directed into the transversal momentum transfer to the projectile and y' perpendicular to the nuclear scattering plane.

The single differential cross section $d\sigma/dp_{r,\mathrm{re}}$ at $v_p = 0.9$ a.u. is displayed in Fig. 5. The most noticeable feature is the close similarity of TI2 and SI2, which are the two processes leading to excited He^+. There is no theoretical work available, which describes this reactions within the molecular orbital approach, but it can be assumed, that at small inter nuclear distances TI2 and SI2 are similar to the mechanism of two electron excitation, which was theoretically investigated by Koike *et al.* [26]. These authors found that the states above the $2p\sigma_u$ auto ionization threshold can be populated from $(2p\sigma_u^2)\,{}^1\Sigma_g^+$, which is correlated diabatically to the initial $He^{2+} + He(1s^2)$ state. The diabatic ${}^1\Sigma_g^+$ is one of the states necessarily needed for the description of the electric scattering and the resonant double electron transfer by only two molecular states. At inter nuclear distance of 0.2 a.u. it is dynamically coupled to states, which cross diabatically the $2p\sigma_u$ continuum. This is essential to reach the $He_2^{3+}(2p\pi) + e^-$ configuration, which consist of the lowest molecular single electron state that converges to $He^{2+} + He(2l)^+$ at the limit of separated atoms. To the best of our knowledge there is no similar promotion to doubly excited stated for the ungerade part of the initial state $(2p\sigma_u, 1s\sigma_g)\,{}^1\Sigma_u^+$. The absence of such a promotion by the ungerade part of the initial state causes equality of TI2 and SI2 within the molecular orbital approach. This is founded in the symmetry of the system in respect to the molecular center.

The location of an electron at one nucleus requires a linear combination of molecular states with different symmetry. This is observed for the two channels where the bound electron is at ground state. While at distant collision i.e. small momentum exchange between the nuclei the electron is perfectly found at the target (SI1) at intermediate impact parameters TI1 dominates. For very close collisions the ratio between these two channels is again inverted. This oscillation structure with the impact parameter is also known for pure electron transfer reactions and indicates that after a hidden crossing promotion the bound electron can end up in the $1s\sigma_g$ as well as the $2p\pi_u$ state.

Information about the molecular symmetry of the emitted electron can be gained from the electron emission pattern. Figure 6 shows the electron velocity distribution projected onto the plane of nuclear motion. For TI1 nodal line structure is found at the beam axis, which is the inter nuclear axis in the initial as well as the final state. This is a

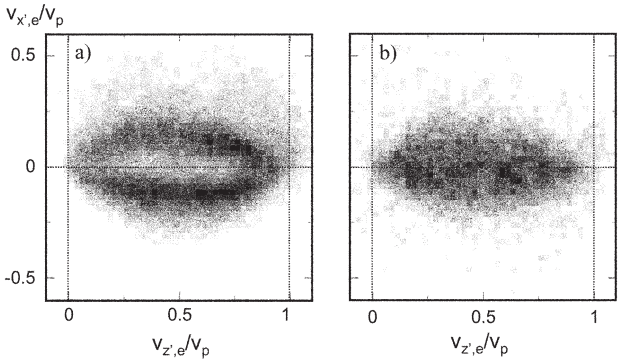

Fig. 6. electron velocity distribution of (a) TI1 and (b) SI1 projected onto the nuclear scattering plane. The horizontal dashed line marks the beam direction, with the projectile velocity at the right and the target at the left vertical line.

clear signature of a promotion mechanism via π states, because rotational coupling can only populate the $p_{x'}$ orientation (nodal plane at $p_{x'} = 0$) of the dipole structure while $p_{y'}$ is forbidden by symmetry conditions. At SI1 the electron emission is concentrated onto the inter-nuclear axis which indicates the dominance of σ states. The underlying physics of this striking difference in the electron emission pattern of TI1 and SI1 can be seen by looking at the transverse momentum exchange (Fig. 5) for these two channels. SI1 happens mainly at such distant collisions where rotation coupling is weak and thereby the contribution of π states is negligible.

5. Conclusion

We have shown that the main features of the experimental observation can be qualitatively understood within the molecular orbital approach. Despite impressive theoretical progress in the treatment of electron transfer between bound states in slow collision by this approach a quantitative prediction of electron emission to the continuum has not been reached. Theoretical results, which show the closest similarity to experimental results, calculate the time evolution of a one-electron wave function on a huge grid either in momentum or configuration [27,28]. These calculations are restricted to single electron problems. Fully differential experimental results are available only for multi electron systems. For such two or more electron systems the correlation between the final state of the bound electron and the structure of the electron emission pattern has to be taken into account, as we have demonstrated here. A quantitative understanding of the electron emission in slow collisions therefore remains a major challenge for the future.

Acknowledgements

This work was supported by DFG, the BMBF, Graduiertenprogramm des Landes Hessen and Roentdek GmbH.

References

1. Fritsch, W., J. Phys. B **27**, 3461 (1994).
2. López, V., Macías, A., Piacentini, R. D., Riera, A. and Yánez, M., J. Phys. B **11**, 2889 (1978).
3. Harel, C. and Salin, A., J. Phys. B **13**, 785 (1980).
4. Gao, R. S. *et al.*, Phys. Rev. A **45**, 6388 (1992).
5. Afrosimov, V. V., Leiko, G. A., Mamaev, Yu. A. and Panov, M. N., Sov. Phys. JETP **40**, 661 (1975).
6. DuBois, R. D., Phys. Rev. A **36**, 2585 (1987).
7. Olson, R. E. *et al.*, Nucl. Instr. Meth. B **124**, 249 (1997).
8. Olson, R. E., Phys. Rev A **27**, 1871 (1983).
9. Irby, V. D. *et al.*, Phys. Rev. A **37**, 3612 (1988).
10. Gay, T. J., Gealy, M. W. and Rudd, M. E., J. Phys. B **23**, L823 (1990).
11. Bernardi, G. C. *et al.*, Phys. Rev. A **40**, 6863 (1989).
12. Bernardi, G., Fainstein, P., Garibotti, C. R. and Suarez, S., J. Phys. B **23**, L139 (1990).
13. Macek, J. H., Ovchinnikov, S. Yu. and Pasovets, S. V., Phys. Rev. Lett. **74**, 4631 (1995).
14. Dörner, R. *et al.*, Phys. Rev. Lett. **77**, 4520 (1996).
15. Ovchinnikov, S. Yu., Macek, J. H., Phys. Rev. Lett. **75**, 2474 (1995).
16. Abdallah, M. A. *et al.*, Phys. Rev. Lett. **81**, 3627 (1998).
17. Abdallah, M. A., Wolff, W., Wolf, H. E., Cocke, C. L. and Stöckli, M., Phys. Rev. A **58**, 3379 (1998).
18. Abdallah, M. A., Wolff, W., Wolf, H. E., Cocke, C. L. and Stöckli, M., J. Phys. B **32**, 4237 (1999).
19. Afaneh, F. *et al.*, J. Phys. B **35**, L229 (2002).
20. Dörner, R. *et al.*, Phys. Reports **330**, 95 (2000).
21. Ullrich, J. *et al.*, Rep. Prog. Phys. **66**, 1463 (2003).
22. Brusdeylins, G., Toennies, J. P., Vollmer, R., XII Symposium Molecular Beams, Book of Abstracts, Perugia, (1989).
23. Mergel, V., Ph.D. thesis, Universität Frankfurt (ISBN 3-8265-2067-X), Shaker Verlag (1996).
24. Dörner, R. *et al.*, Nucl. Instr. Meth. B **124**, 225 (1997).
25. Pedersen, J. O. P. and Hvelplund, P., Phys. Rev. Lett. **62**, 2373 (1989).
26. Koike, F. *et al.*, Phys. B **11**, 4193 (1978).
27. Schultz, D. R., Reinhold, C. O., Krsti'c, P. S. and Strayer, M. R., Phys Rev. A **65**, 52722 (2002)
28. Chassid, M. and Horbatsch, M., Phys. Rev. A **66**, 12714 (2002).

